DATA-DRIVEN CLUSTER SELECTION FOR SUBCORTICAL SHAPE AND CORTICAL THICKNESS PREDICTS RECOVERY FROM DEPRESSIVE SYMPTOMS

Benjamin S.C. Wade[1,3], Jing Sui[2], Stephanie Njau[1], Amber M. Leaver[1], Megha Vasvada[1], Boris A. Gutman[3], *Paul M. Thompson[3], Randal Espinoza[4], Roger P. Woods[1], Christopher C. Abbott[5], Katherine L. Narr[1], Shantanu H. Joshi[1]*

[1]Ahmanson-Lovelace Brain Mapping Center, Department of Neurology, UCLA [2]The Mind Research Network and Lovelace Biomedical and Environmental Research Institute, Albuquerque, NM [3]Imaging Genetics Center, USC [4]Department of Psychiatry and Biobehavioral Sciences, UCLA [5]Department of Psychiatry, University of New Mexico

ABSTRACT

Patients with major depressive disorder (MDD) who do not achieve full symptomatic recovery after antidepressant treatment have a higher risk of relapse. Compared to pharmacotherapies, electroconvulsive therapy (ECT) more rapidly produces a greater extent of response in severely depressed patients. However, prediction of which candidates are most likely to improve after ECT remains challenging.

Using structural MRI data from 42 ECT patients scanned prior to ECT treatment, we developed a random forest classifier based on data-driven shape cluster selection and cortical thickness features to predict remission. Right hemisphere hippocampal shape and right inferior temporal cortical thickness was most predictive of remission, with the predicted probability of recovery decreasing when these regions were thicker prior to treatment. Remission was predicted with an average 73% balanced accuracy. Classification of MRI data may help identify treatment-responsive patients and aid in clinical decision-making. Our results show promise for the development of personalized treatment strategies.

Index Terms— Random Forest, treatment response prediction, shape analysis, major depression, electroconvulsive therapy

1. INTRODUCTION

About 16 million (6.9%) US adults suffer from at least one major depressive episode in a given year. Global 12-month prevalence rates are similar (~6 %), though vary regionally [1]. Despite available therapies, only a minority (20-40%) of individuals will achieve full symptomatic remission after initial or successive treatment attempts. Unfortunately, residual symptoms increase the risk of relapse [2], and with the recurrence of depressive episodes, symptoms become more refractory over time. The ability to predict the probability of therapeutic response would decrease the need for multiple lengthy medication trials, which appear needed in about 50% of patients [3], reduce suffering and enhance clinical outcomes. Several recent studies suggest that brain features extracted from structural neuroimaging data might relate to and predict symptom improvement [4, 5]. However, prognostic markers of post-treatment remission have not yet been identified.

Electroconvulsive therapy (ECT), an established treatment typically reserved for severe depression, works more quickly (response can occur in 2-4 weeks) and has higher remission rates than other standard therapeutic approaches [6]. The fast acting and robust clinical effects of ECT make this treatment ideal for determining whether structural variations in the brain might predict individual recovery from depression after completing a series of treatments. The existing neuroimaging literature suggests brain abnormalities in prefrontal and temporal cortical association regions as well as subcortical hippocampal, amygdalar, thalamic, ventral striatal/pallidal, and brainstem centers are of high relevance to the pathophysiology of major depressive disorder (MDD) [7]. We and others have further shown that changes in these regions or networks occur with ECT [8-13]. However, few prior studies have simultaneously investigated whether regional changes in volume, shape and/or gray matter thickness might predict recovery from symptoms.

In this paper, we propose an unbiased data-driven approach applied to morphometric feature extracted from regions across the brain, including those not expected to link with depression, to determine if variations in these features might serve as prognostic markers for future remission following ECT. Additionally, we present a novel shape-based feature selection approach that defines clusters of shape features based on associations between shape and change in symptom severity over treatment. This approach has the benefit of preserving local information about a region's shape while simultaneously reducing the dimensionality of the feature set and the computational complexity. Unlike previously developed patch-based approaches [14, 15] that have used either neighborhood similarity metric or SPHARM coefficients for feature selection, our method achieves shape cluster learning by optimizing the remission classification performance related to change in depression mood scores. To our knowledge this is the first time that such an approach has been used for prediction of remission in depression.

2. MATERIALS AND METHODS

978-1-5090-1172-8/17/$31.00 ©2017 IEEE

2.1 Participants

42 patients from the University of California, Los Angeles (mean age, 41 years [SD 14 years]; range 19 - 74) all experiencing a DSM-IV defined major depressive episode and eligible to receive ECT were recruited as part of an ongoing study investigating treatment responsive biomarkers for antidepressant response in MDD. Patients were evaluated at two time points: 24 hours prior to ECT (T1) and within a week of completing ECT index (T2).

The Hamilton Depression Rating Scale (HAM-D-17) [16] was used to assess depression severity at each time point. Participants having a HAM-D-17 score of 8 or less at T2 were labeled remitters [17]. 13 Patients remitted following ECT. The study protocol was approved by the Institutional Review Board at UCLA.

2.2 Image acquisition and segmentation

High-resolution motion-corrected multi-echo T1-weighted MPRAGE structural brain images [18] were acquired on a Siemens 3T Allegra system (Erlangen, Germany) for all subjects and time points (TEs/TR= 1.74, 3.6, 5.46, 7.32/2530 ms, TI=1260 ms, flip angle=7°, voxel resolution = 1.3×1×1 mm^3).

Previously validated FreeSurfer [19] workflows, which include removal of non-brain tissue, intensity normalization and automated volumetric parcellation based on probabilistic information from manually labeled training sets, were used for whole brain cortical (Desikan Killiany atlas-based parcellations) and subcortical segmentation. Segmentations were visually inspected and corrected for topographic errors where needed.

2.3 Candidate features

Cortical thickness of 70 regions of interest (ROIs) and volumes of 14 subcortical ROIs were estimated from FreeSurfer segmentations. The local thickness (i.e. shape) values of the 14 subcortical structures, including the bilateral accumbens, amygdala, caudate, hippocampus, pallidum, putamen and thalamus, were further estimated using the Medial Demons framework described in [20]. In short, following non-linear warping to a spherical probabilistic template, local thickness of each subcortical surface was computed as the shortest distance from each vertex with respect to a skeletonized medial core traversing the anterior-posterior axis of the structure. This local thickness for each mesh was represented at each of the vertices whose number scaled roughly with the average volume. Depending on the ROI, the resolution of each mesh ranged from 900 to 2500 amounting to 27,120 vertices in total. Age was also included as a candidate feature due to its well-known association with brain morphometry and neural integrity.

2.4 Data driven subcortical shape cluster selection

To reduce the dimensionality of the feature set and preserve the ability to report on clinically informative subregions of a subcortical surface, we defined clusters of vertices and estimated the average cluster-level local thickness. Shape clusters of vertices were defined within the training set of each classification fold

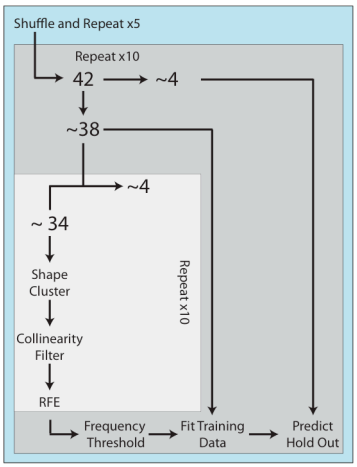

Fig. 1. Flowchart of classification process.

based on the two criteria: i) their individual, training fold subject-wise correlation with the percent of change in HAM-D-17 score between the two scan times T1 and T2 ($\frac{HAMD\ T1-HAMD\ T2}{HAMD\ T1} = \Delta HAMD$) was above a threshold r_{thresh} and ii) the vertices with $|r| \geq r_{thresh}$ comprised a connected neighborhood cluster extent (CE) $\geq$ a threshold CE_{thresh} where $r_{thresh} \in \{0.025, 0.05, 0.1, 0.15, 0.2\}$ and $CE_{thresh} \in \{10, 20, 50, 100\}$. The effects of these parameterizations on classification performance were determined empirically via nested cross-validation described in section 2.6. The number and extent of shape clusters necessarily varied at each fold. Clusters identified in training folds were mapped to participants in testing folds and recomputed for cross-validation. Cortical thickness and subcortical volume measures were not subject to filtering as they contributed far less to feature set dimensionality.

2.5 Random forest classifier

Our classifier of choice was a random forest (RF) which is a supervised classifier built on an ensemble of classification and regression trees (CART) [21] where each CART is composed of bootstrapped sample cases. Each decision node, v, within a CART is given a random subset of features for which the Gini impurity index is calculated as,

$$Gini(v) = \sum_{c=1}^{C} \hat{p}_c^v\ (1 - \hat{p}_c^v), \tag{1}$$

where $\hat{p}_c^v$ is the proportion of cases in class c at node v. CART nodes are split by the feature X_i maximizing the class purity of its child nodes, v^r and v^l by selecting the maximum $Gain\ (X_i, v)$ given by,

$$Gain\ (X_i, v) = Gini(X_i, v) - \omega_l Gini(X_i, v^l) - \omega_r Gini(X_i, v^r), \tag{2}$$

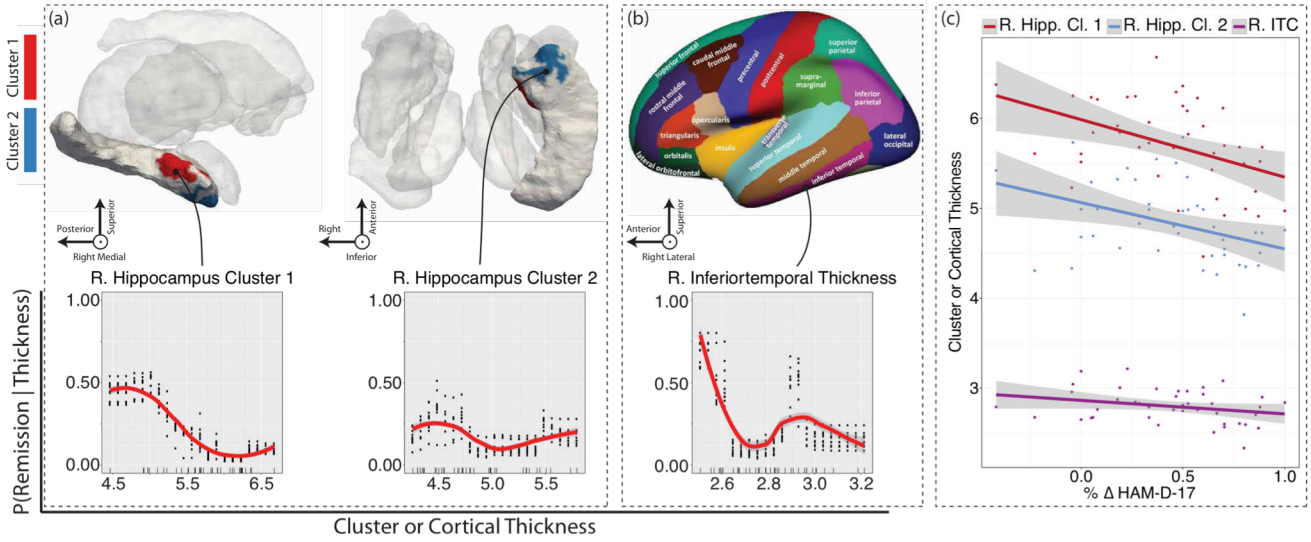

Fig. 2. Illustration of shape clusters (a) and cortical (b) ROIs (top) most important in the prediction of remission. Line plots (bottom) indicate the predicted probability of remission over an observed range (minimum to maximum in 20 even increments) of ROI thicknesses averaged across 10 bootstrapped resamples of the data set and refitted to the derived classifier. A non-parametric LOESS model was fit to the predicted responses. Points about each line indicate predicted probabilities from each resample while rugs of each plot indicate the density of observed values in the whole sample. Note that orientation axes are provided below (a-b) as these are in radiological orientation (left-right flipped). (c) Plots least squares fits between the percent change in HAM-D-17 scores and baseline ROI thickness.

where ω_l and ω_r are the proportions of cases in node v assigned to child nodes v^r and v^l. The global importance I of feature X_i is taken as the summation of the decreases in the Gini coefficient at each node partitioned by X_i. Specifically,

$$I_{X_i} = \frac{1}{total\ tree\ number} \sum_{v \in S_{X_i}} Gain(X_i, v), \quad (3)$$

where S_{X_i} is the set of nodes split by X_i. RFs grow each CART to its full extent and determine the label of a new observation by majority vote of its constituent terminal nodes. Each RF was tuned using a grid search over the number of variables passed to each node from 2 to p, where p is the number of variables in the feature set. The constituent number of CARTs in each forest was 1000.

2.6 Nested cross-validation and feature selection

To further randomize subjects used for training and testing, we implemented a nested cross-validation approach, where the outermost loop performs error-averaging by repeating the experiment 5 times. At each iteration participants were randomly reassigned to one of 10 cross validation folds to stratify the training and disjoint hold-out datasets, while the inner most loop performs feature selection by further partitioning the subjects into 10 sub-folds and using them independently for feature selection. **Figure 1** illustrates the joint nested cross validation and feature selection process. The feature selection process used participants in 9 of the 10 sub-folds to define candidate shape clusters. Highly collinear features were removed if two features were correlated above a threshold ρ_{thresh} where $\rho_{thresh} \in \{0.5, 0.6, 0.7\ 0.8, 0.9, 0.95\}$. Of the two highly correlated features, the one with the largest absolute correlation with all other features was removed from the feature set. Features surviving this initial threshold were then evaluated using 10-fold recursive feature elimination (RFE) [22] where the internal classifier was also a RF composed of 1000 trees. The RFE algorithm proceeded by fitting a RF using all features and computing the importance (equation 3) of each feature in the full model. P feature subsets of sizes 1:P were created where P was the number of features surviving ρ_{thresh}. For all subsets, S_i, $i = 1{:}P$, the 1:i-th most important features were used to predict remission status with a RF. The feature set yielding the highest average accuracy across all 10 RFE folds was selected. RFE and all RF models were fit using the caret package in R [23].

As shown in Figure 1, the RFE process was repeated for all ten nested folds. Upon completion of the internal folds, we evaluated the frequency of a feature's occurrence in the optimal RFE subset and retained only those occurring with a frequency $f \geq f_{thresh}$ where $f_{thresh} \in \{0.2, 0.3, \ldots, 1\}$ is defined relatively as the j-th quantile of frequencies of an ROI's occurrence in the optimal feature set. f_{thresh} was necessarily defined at the vertex level for shape features. Vertices and individual ROIs surviving this thresholding process were subsequently used as features for prediction of the entire training set. Surviving vertices were re-clustered, and required to have CE $\geq CE_{thresh}$ (where CE_{thresh} is the same threshold used for initial cluster formation) and within cluster thickness averages were recomputed. Importantly, testing observations did not contribute to the feature selection process. Using a grid search we explored the space of all possible parameter combinations, r_{thresh}, CE_{thresh}, ρ_{thresh} and f_{thresh} resulting in a total of 1080 candidate parameterizations. Performances were averaged across all 5 repetitions of this process.

The prevalence of non-remitters was 69%; the baseline detection rate. Accuracy measures in binary classification problems with imbalanced samples are known to be biased towards the more prevalent class. To avoid inflated performance metrics we report on the balanced accuracy (BA) [24] defined as the average

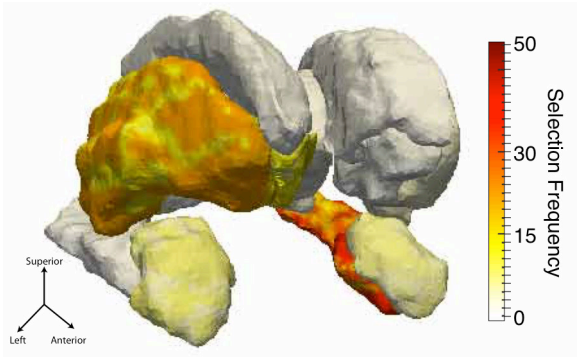

Fig. 3. Vertex selection frequency

accuracy across both classes, formally BA = $\frac{1}{2}(\frac{True\ Positive}{Positive} + \frac{True\ Negative}{Negative})$. Our outermost loop allows us to further estimate the uncertainty of our performance estimates which is important given the increased likelihood of arriving at an accurate solution by chance in our large parameter space.

3. RESULTS

3.1 Model performance

We selected the model parameterization yielding the highest average test BA across all 5 repeated folds. The highest BA was given by the parameters r_{thresh} = 0.025, CE_{thresh}, = 10 ρ_{thresh} = 0.95 and f_{thresh} = 1 resulting in a mean BA = 73% (range 64-79%), accuracy = 78% (range 61-83%), sensitivity = 85% (range 79-89%), specificity = 61% (range 46-69%), positive predictive value = 83% (range 77-86%), negative predictive value = 65% (range 54-75%) where non-remitters were the positive class.

Under this parameterization there were an average of 4 (SD = 2) features selected at each fold. The frequency of a feature's selection across cross validation folds is directly related to its overall importance by equation 3. Three features were selected in at over half (≥ 60%) of the models and therefore considered most important in predicting remission: two shape clusters of the right anterior hippocampus and the cortical thickness of the right inferior temporal cortex (ITC).

3.2 Associations between morphometry and clinical outcome

In order to understand the relationship between these regions and the predicted probability of a patient's remission, we fit a RF to 10 bootstrapped resamples of the patients using only these ROIs. **Figure 2**(a-b) illustrates this by plotting the predicted probability a hypothetical patient experiences symptom remission given an observed range of values (from minimum to maximum) in 20 even increments for each ROI while holding other ROIs at their respective observed means. A non-parametric LOESS model was fit to the resampled predicted probabilities. The predicted probability of remission declined sharply as the thickness of the right ITC and hippocampal clusters increased.

As a *post hoc* analysis we tested the correlation between the thickness of these regions and $\Delta HAMD$. Figure 2(c) plots the linear least squares fit of these associations. $\Delta HAMD$ was significantly anticorrelated with the first (r = -0.43, p = 0.004) and second (-0.38, p = 0.01) hippocampal clusters but not with ITC thickness (-0.27, p = 0.08). The significance of these associations survived correction for multiple comparisons using the standard 5% false discovery rate.

Additional shape clusters from several regions involved in emotional response and reward circuitry and affected by MDD were selected with moderate frequencies including the bilateral amygdala (12%), left putamen (36%) and accumbens (22%). The frequency of each vertices' selection is shown in **Figure 3**. No other regions were selected in over 10% of the folds; age was never selected suggesting it was not a critical factor.

4. DISCUSSION

A primary aim in prognostic pattern recognition is the stratification of patients into groups likely and unlikely to benefit from a course of treatment. Remission, which leads to a better long term prognosis [2], is the ultimate goal of treatment. Identifying which individuals will make a full symptomatic recovery following ECT or any other antidepressant treatment will aid clinicians in determining optimal treatment strategies and help patients and their health care providers anticipate and manage future relapse risk. Using a large cohort of ECT patients from UCLA, we thus sought to identify prognostic biomarkers of remission from pre-treatment MRI scans.

Right hemisphere temporal lobe structures were most predictive of remission. These regions are biologically plausible since reduced hippocampal volume is widely implicated in the neuropathology of depression [7, 25] while the ITC is a center of integration for mood and emotional stimuli [26]. ECT has previously been demonstrated to induce neuroplastic changes in both structures [12, 27]. We further probed our classifier to build a profile of regional characteristics indicative of remission. The predicted probability of remission was largely inversely associated with the thickness of these regions in our random forest classifier and subsequent tests of correlation confirmed that $\Delta HAMD$ was significantly anticorrelated with the baseline thickness of these regions.

This finding is consistent with several prior reports showing increased hippocampal volume with ECT [12, 28] and our prior finding of a moderate relationship between smaller hippocampal volume at baseline and greater improvement in clinical response in an overlapping sample [12]. However, this is somewhat in opposition to a recent meta-analysis that reported reduced hippocampal volumes associated with lower remission likelihood to antidepressant drug therapies [29] though different mechanisms may occur for brain stimulation versus pharmacological interventions. It is also noteworthy that 83% of the ECT lead placements in our study were right unilateral (placed over the right temporal area) which is ipsilateral to both the right ITC and right hippocampus. This may suggest that clinical outcome is partially determined by an interaction between the proximity of these structures to the induced current and their morphometry at the time of treatment. Future work will develop models that generalize across independent sites. Our current findings are encouraging and suggest that data-driven models based on neuroimaging may inform personalized treatment strategies.

5. REFERENCES

[1] R. C. Kessler and E. J. Bromet, "The epidemiology of depression across cultures," *Annu Rev Public Health,* vol. 34, pp. 119-38, 2013.

[2] M. B. Keller, "Remission versus response: the new gold standard of antidepressant care," *J Clin Psychiatry,* vol. 65 Suppl 4, pp. 53-9, 2004.

[3] B. N. Gaynes, D. Warden, M. H. Trivedi, S. R. Wisniewski, M. Fava, and A. J. Rush, "What did STAR*D teach us? Results from a large-scale, practical, clinical trial for patients with depression," *Psychiatr Serv,* vol. 60, pp. 1439-45, Nov 2009.

[4] M. L. Phillips, H. W. Chase, Y. I. Sheline, A. Etkin, J. R. Almeida, T. Deckersbach*, et al.*, "Identifying predictors, moderators, and mediators of antidepressant response in major depressive disorder: neuroimaging approaches," *Am J Psychiatry,* vol. 172, pp. 124-38, Feb 1 2015.

[5] F. Ten Doesschate, P. van Eijndhoven, I. Tendolkar, G. A. van Wingen, and J. A. van Waarde, "Pre-treatment amygdala volume predicts electroconvulsive therapy response," *Front Psychiatry,* vol. 5, p. 169, 2014.

[6] M. M. Husain, A. J. Rush, M. Fink, R. Knapp, G. Petrides, T. Rummans*, et al.*, "Speed of response and remission in major depressive disorder with acute electroconvulsive therapy (ECT): a Consortium for Research in ECT (CORE) report," *J Clin Psychiatry,* vol. 65, pp. 485-91, Apr 2004.

[7] W. C. Drevets, J. L. Price, and M. L. Furey, "Brain structural and functional abnormalities in mood disorders: implications for neurocircuitry models of depression," *Brain Struct Funct,* vol. 213, pp. 93-118, Sep 2008.

[8] J. S. Pirnia T, Khalil J, Leaver A, Woods RP, Espinoza R, Narr KL, "Electroconvulsive therapy and structural neuroplasticity in neocortical, limbic and paralimbic cortex," *Transl Psychiatry,* vol. 6, p. e832, 2016.

[9] S. Njau, S. Joshi, A. M. Leaver, M. Vasavada, J. van Fleet, R. Espinoza*, et al.*, "Variations in myo-inositol in fronto-limbic regions and clinical response to electroconvulsive therapy in major depression," *Journal of Psychiatric Research,* vol. 80, pp. 45-51, 2016.

[10] A. M. Leaver, R. Espinoza, T. Pirnia, S. H. Joshi, R. P. Woods, and K. L. Narr, "Modulation of intrinsic brain activity by electroconvulsive therapy in major depression," *Biological Psychiatry: Cognitive Neuroscience and Neuroimaging,* vol. 1, pp. 77-86, 2016.

[11] A. M. Leaver, R. Espinoza, S. H. Joshi, M. Vasavada, S. Njau, R. P. Woods*, et al.*, "Desynchronization and Plasticity of Striato-frontal Connectivity in Major Depressive Disorder," *Cereb Cortex,* Sep 22 2016.

[12] S. H. Joshi, R. T. Espinoza, T. Pirnia, J. Shi, Y. Wang, B. Ayers*, et al.*, "Structural Plasticity of the Hippocampus and Amygdala Induced by Electroconvulsive Therapy in Major Depression," *Biol Psychiatry,* vol. 79, pp. 282-92, Feb 15 2016.

[13] B. S. Wade, S. H. Joshi, S. Njau, A. M. Leaver, M. Vasavada, R. P. Woods*, et al.*, "Effect of Electroconvulsive Therapy on Striatal Morphometry in Major Depressive Disorder," *Neuropsychopharmacology,* Apr 12 2016.

[14] P. Yushkevich, S. Joshi, S. M. Pizer, J. G. Csernansky, and L. E. Wang, "Feature selection for shape-based classification of biological objects," *Inf Process Med Imaging,* vol. 18, pp. 114-25, Jul 2003.

[15] E. Gerardin, G. Chetelat, M. Chupin, R. Cuingnet, B. Desgranges, H. S. Kim*, et al.*, "Multidimensional classification of hippocampal shape features discriminates Alzheimer's disease and mild cognitive impairment from normal aging," *Neuroimage,* vol. 47, pp. 1476-86, Oct 1 2009.

[16] M. Hamilton, "A rating scale for depression," *J Neurol Neurosurg Psychiatry,* vol. 23, pp. 56-62, Feb 1960.

[17] M. B. Keller, "Past, present, and future directions for defining optimal treatment outcome in depression: remission and beyond," *JAMA,* vol. 289, pp. 3152-60, Jun 18 2003.

[18] A. J. van der Kouwe, T. Benner, D. H. Salat, and B. Fischl, "Brain morphometry with multiecho MPRAGE," *Neuroimage,* vol. 40, pp. 559-69, Apr 1 2008.

[19] A. M. Dale, B. Fischl, and M. I. Sereno, "Cortical surface-based analysis. I. Segmentation and surface reconstruction," *NeuroImage,* vol. 9, pp. 179-94, Feb 1999.

[20] B. Gutman, Y. Wang, P. Rajagopalan, A. Toga, and P. Thompson, "Shape matching with medial curves and 1-D group-wise registration," *International Symposium on Biomedical Imaging,* vol. 9, pp. 716-719, 2012.

[21] L. Breiman, "Random Forests," *Machine Learning,* vol. 45, pp. 5-32, 2001/10/01 2001.

[22] M. Xi, J. Sun, L. Liu, F. Fan, and X. Wu, "Cancer Feature Selection and Classification Using a Binary Quantum-Behaved Particle Swarm Optimization and Support Vector Machine," *Comput Math Methods Med,* vol. 2016, p. 3572705, 2016.

[23] M. Kuhn, "Building Predictive Models in R Using the caret Package," *2008,* vol. 28, p. 26, 2008-11-10 2008.

[24] K. H. Brodersen, C. S. Ong, K. E. Stephan, and J. M. Buhmann, "The Balanced Accuracy and Its Posterior Distribution," *Proceedings of ICPR '10 Proceedings of the 2010 20th International Conference on Pattern Recognition,* pp. 3121-3124.

[25] L. Schmaal, D. J. Veltman, T. G. van Erp, P. G. Samann, T. Frodl, N. Jahanshad*, et al.*, "Subcortical brain alterations in major depressive disorder: findings from the ENIGMA Major Depressive Disorder working group," *Mol Psychiatry,* vol. 21, pp. 806-12, Jun 2016.

[26] D. A. Seminowicz, H. S. Mayberg, A. R. McIntosh, K. Goldapple, S. Kennedy, Z. Segal*, et al.*, "Limbic-frontal circuitry in major depression: a path modeling metanalysis," *Neuroimage,* vol. 22, pp. 409-18, May 2004.

[27] T. Pirnia, S. H. Joshi, A. M. Leaver, M. Vasavada, S. Njau, R. P. Woods*, et al.*, "Electroconvulsive therapy and structural neuroplasticity in neocortical, limbic and paralimbic cortex," *Transl Psychiatry,* vol. 6, p. e832, Jun 07 2016.

[28] C. C. Abbott, T. Jones, N. T. Lemke, P. Gallegos, S. M. McClintock, A. R. Mayer*, et al.*, "Hippocampal structural and functional changes associated with electroconvulsive therapy response," *Transl Psychiatry,* vol. 4, p. e483, 2014.

[29] R. Colle, I. Dupong, O. Colliot, E. Deflesselle, P. Hardy, B. Falissard*, et al.*, "Smaller hippocampal volumes predict lower antidepressant response/remission rates in depressed patients: A meta-analysis," *World J Biol Psychiatry,* pp. 1-8, Aug 15 2016.